Organic Geochemistry 92 (2016) 32–41

Contents lists available at ScienceDirect

Organic Geochemistry

journal homepage: www.elsevier.com/locate/orggeochem

Weathering of pyrogenic organic matter induces fungal oxidative enzyme response in single culture inoculation experiments

Christy Gibson [a], Timothy D. Berry [a], Ruzhen Wang [a,b], Julie A. Spencer [c], Cliff T. Johnston [d], Yong Jiang [b], Jeffrey A. Bird [e,f], Timothy R. Filley [a,d,*]

[a] Department of Earth, Atmospheric, and Planetary Sciences and the Purdue Climate Change Research Center, Purdue University, West Lafayette, IN 47907, USA
[b] State Key Laboratory of Forest and Soil Ecology, Institute of Applied Ecology, Chinese Academy of Sciences, Shenyang 110016, China
[c] Department of Chemistry, Johns Hopkins University, Baltimore, MD 21218, USA
[d] Department of Agronomy, Purdue University, West Lafayette, IN 47907, USA
[e] School of Earth and Environmental Sciences, Queens College, City University of New York, Flushing, NY 11367, USA
[f] Earth and Environmental Sciences PhD Program, The Graduate Center, City University of New York, New York, NY 10016, USA

ARTICLE INFO

Article history:
Received 21 May 2015
Received in revised form 30 November 2015
Accepted 2 December 2015
Available online 12 December 2015

Keywords:
^{13}C
Pyrogenic organic matter
Fungal decomposition
Enzyme
Phenol oxidase
Peroxidase
Priming

ABSTRACT

The addition of pyrogenic organic matter (PyOM), the aromatic carbon-rich product of the incomplete combustion of plant biomass or fossil fuels, to soil can influence the rate of microbial metabolism of native soil carbon. The interaction of soil heterotrophs with PyOM may be governed by the surficial chemical and physical properties of PyOM that evolve with environmental exposure. We present results of a 36-day laboratory incubation investigating the interaction of a common white-rot fungus, *Trametes versicolor*, with three forms of ^{13}C-enriched (2.08 atom% ^{13}C) PyOM derived from *Pinus ponderosa* (450 °C): one freshly produced, and two artificially weathered (254 nm, UV light-water treatment and water-leaching alone). Analysis (FTIR, XPS) of the UV-weathered PyOM showed increased aliphatic C–H content and oxidation of aromatic carbon relative to both the original and water-leached PyOM. The addition of both weathered forms of PyOM stimulated (positively primed) fungal respiration of the growth media, while the unaltered PyOM mildly inhibited (negatively primed) respiration. Artificial weathering resulted in higher oxidative (laccase and peroxidase) enzyme activity than unaltered PyOM, possibly the result of a diminished capacity to bind reactive substrates and extracellular enzymes after weathering. However, and contrary to expectations, simple water-leached weathering resulted in a relatively higher enzyme activity and respiration than that of UV-weathering. The ^{13}C content of respired CO_2 indicated negligible fungal oxidation of PyOM for all treatments, demonstrating the overall low microbial reactivity of this high temperature PyOM. The increased enzymatic and positive priming response of *T. versicolor* to weathered PyOM highlights the importance of weathering-induced chemistry in controlling PyOM–microbe–soil carbon interactions.

1. Introduction

Pyrogenic organic matter (PyOM), the solid, aromatic, carbon-rich product of the incomplete combustion of plant biomass or fossil fuels, can exert many important influences on terrestrial ecosystem dynamics through its alteration of the chemical, physical, and microbiological properties of soil (Hammes and Schmidt, 2009; Lehmann et al., 2009; Hart and Luckai, 2013). PyOM can make up a significant proportion (~5–45%) of soil organic carbon (SOC) (Glaser et al., 1998; Skjemstad et al., 1996, 2002; Schmidt et al., 1999) with estimates as high as 89% of SOC in some desert and urban soils (Hamilton and Hartnett, 2013). The mean residence time (MRT) of biomass-derived PyOM C in soil is much higher than its unpyrolyzed source material (Santos et al., 2012; Maestrini et al., 2014b). Six-month laboratory soil mesocosms of ponderosa pine-derived PyOM showed microbial decay losses of ~0.4% compared with 30% C loss of its parent pine material (Santos et al., 2012).

Abbreviations: FTIR, Fourier transform infrared spectroscopy; DR-FTIR, diffuse reflectance Fourier transform infrared spectroscopy; NMR, nuclear magnetic resonance spectroscopy; MEA, malt extract agar; PYOM, pyrogenic organic matter; XPS, X-ray photoelectron spectroscopy; HCAC, highly condensed aromatic carbon.

* Corresponding author at: Department of Earth, Atmospheric, and Planetary Sciences and the Purdue Climate Change Research Center, Purdue University, West Lafayette, IN 47907, USA. Tel.: +1 765 494 6581.
E-mail address: filley@purdue.edu (T.R. Filley).

http://dx.doi.org/10.1016/j.orggeochem.2015.12.003
0146-6380/

MRTs of PyOM are typically on the centennial scale although a broader range, ~90–1616 years, has been reported (Singh et al., 2012). This "recalcitrance" imparted to biomass carbon is based upon an enhanced resistance to microbial decay derived from thermodynamic, structural, and inhibitory controls (i.e., high hydrophobicity, high aromaticity and condensation, and potentially toxic gaseous or extractive chemicals) (Hammes et al., 2008). The potential for enhanced C sequestration by PyOM in soil, in addition to positive influences to cation exchange capacity, pH, and enhanced microbial nutrient cycling, is one of the asserted positive benefits for the intentional production and addition of PyOM or biochar to agricultural soils, although a beneficial response to soil has not been consistently observed (Lehmann et al., 2006; McHenry, 2009; Laird et al., 2010a,b; Kauffman et al., 2014). The impact that increased PyOM input to surface soils will have in forest ecosystems experiencing greater frequency and intensity of forest fires is still being debated (Adams, 2013).

As stable as PyOM seems to be under natural soil conditions, it is, however, susceptible to environmental oxidative alteration by both biotic and abiotic factors (Kawamoto et al., 2005; Cheng et al., 2006; Zimmerman, 2010; LeCroy et al., 2013). PyOM may be susceptible to oxidation in the dark under aqueous conditions (Zimmerman, 2010), by interaction with ozone (Kawamoto et al., 2005), and on contact with air (Cohen-Ofri et al., 2006), demonstrating that PyOM can be progressively weathered by natural abiotic processes in soil or while entrained in the atmosphere (Cheng et al., 2006). Generation of an oxidative rind (LeCroy et al., 2013) can influence its wettability, solubility, and porosity and thus the ability of microbes to both inhabit and utilize it as a carbon source (Hockaday et al., 2006; Lehmann et al., 2011).

It is estimated that over 7.6 Tg of particulate PyOM is emitted into the atmosphere globally with 42% contributed from open biomass burning (Bond et al., 2013). Recent studies, however, have shown that global emission values may be underestimated by a factor of 3 (Randles et al., 2013) and that rural emission contribution to this estimate is very low (Santos et al., 2014). PyOM particles can persist in the atmosphere on a time scale of days to weeks and can travel long distances prior to deposition (Environmental Protection Agency, 2012; Santos et al., 2014) as is evidenced by the influence of PyOM on the albedo and subsequent melting of Arctic glaciers (Clarke and Noone, 1985). It is unknown exactly how much PyOM is redeposited from the atmosphere and is incorporated in soil but estimates place it between <1% and 17% of SOC (Hamilton and Hartnett, 2013; Santos et al., 2014; Lehndorff et al., 2015). Photolytic oxidation of PyOM, either at the surface of the soil or once entrained as particulate matter in the atmosphere, could be extensive, particularly where UV exposure is high (Khalizov et al., 2009). Once oxidized to produce soluble PyOM, fractions of this material may further react photolytically or, once in the soil or aquatic system, be metabolized by microbes or bind to particle surfaces (Kuhlbusch, 1998; Hockaday et al., 2006; Fujii et al., 2009). However, current estimates of PyOM MRT do not consider the potential effects of photochemical oxidation or environmental weathering on its fate.

The addition of PyOM to soil can influence the stability of native soil carbon by increasing (positive priming) or decreasing (negative priming) rates of microbial metabolism (Hamer et al., 2004; Liang et al., 2010; Zimmerman et al., 2011; Maestrini et al., 2014a). However, the magnitude and direction of the priming effect can vary with soil and PyOM type, addition rate, incubation conditions, and length of study (e.g., Zimmerman et al., 2011; Santos et al., 2012; Woolf and Lehmann, 2012). In soil incubations, positive priming effects are often observed in the initial stages of the experiment which are subsequently followed by a trend to negative or neutral priming. This trend has been attributed to an initial co-metabolism of labile fractions within PyOM and SOC (Hamer et al., 2004; Cheng and Lehmann, 2009; Jones et al., 2011; Keith et al., 2011; Zimmerman et al., 2011; Maestrini et al., 2014a). Negative priming effects have been attributed to physical and chemical protection mechanisms such as sorption of dissolved organic matter to PyOM surfaces, or accumulation of the more recalcitrant portion of the PyOM after the labile materials are decomposed (Bell and Worrall, 2011; Jones et al., 2011; Zimmerman et al., 2011; Singh et al., 2012; Farrell et al., 2013). More recently, the potential for PyOM to disrupt intracellular signaling of specific microbial groups has been posited as a phenomenon contributing to negative priming effects (Masiello et al., 2013).

Field and laboratory PyOM incubations have recently demonstrated that a wide range of soil microbe groups have the ability to assimilate and oxidize PyOM in soil (Santos et al., 2012; Farrell et al., 2013; Gomez et al., 2014). Saprotrophic wood decay fungi are considered to have an enhanced capacity to degrade many forms of highly condensed aromatic carbon (HCAC) given the complement of extracellular phenoloxidases and peroxidases they produce. In particular, many forms of white-rot decay fungi, such as *Trametes versicolor*, are known to degrade and take up many forms of HCAC including manufactured fullerol nanocarbon, PAHs, and coal products (Hofrichter et al., 1999; Márquez-Rocha et al., 2000; Leonowicz et al., 2001; Andersson et al., 2003; Schreiner et al., 2009). Recent decay studies of highly condensed aromatic nanocarbon materials (e.g., carbon nanotubes, fullerols) indicate that surface oxidation, as would be induced through chemical, biological, or photolytic oxidation (i.e., weathering that adds hydroxyl or carboxyl groups) greatly increases the metabolic response of saprophytic soil fungi (Schreiner et al., 2009; Berry et al., 2014). Knowledge of how specific microbial groups, like saprotrophic fungi or other potential degraders, respond to the presence of different weathering states of HCAC may be an important key to understanding both the short and long term ecological impact of PyOM in soils.

We present the results of a 36-day laboratory single culture incubation study investigating the interaction of a common saprotrophic white-rot fungus, *T. versicolor*, with artificially weathered (both 254 nm light in a water slurry and water leached) and unaltered 450 °C PyOM produced from ^{13}C-enriched (3 atom% ^{13}C) *Pinus ponderosa*. We hypothesized that the photolytically weathered PyOM will enhance the C mineralization of the malt extract agar (MEA) growth media (i.e., positive priming) compared with untreated PyOM. Similarly, we also expected greater enzymatic oxidation of the photolytically weathered PyOM resulting in the production of measurable ^{13}C-labeled CO_2. In contrast, we expect that PyOM that is unaltered or simply weathered through water leaching will exhibit little inductive or primary reactivity given its higher degree of condensed aromatic surface chemistry, lower surface oxidation, and decreased solubility of low molecular components. We quantified the decomposition of culture growth media and PyOM by monitoring the isotopic CO_2 efflux and carbon isotopic composition, and the influence of PyOM on fungal enzymatic response by measuring the activity of the oxidative enzymes laccase and peroxidase.

2. Materials and methods

2.1. Production of PyOM

Detailed description of the methods to grow Ponderosa pine, *P. ponderosa*, saplings under ^{13}C–CO_2 atmosphere and the subsequent pyrolysis were given in Bird and Torn (2006) and Santos et al. (2012). Briefly, *P. ponderosa* saplings were grown in a chamber with a pulsed $^{13}CO_2$ atmosphere, at the University of California, Davis. Stems were then pyrolyzed at a constant temperature of

450 °C for 5 h under N_2 with the resultant PyOM characterized using solid state ^{13}C NMR, and elemental and stable isotope analysis (Santos et al., 2012). The stable carbon isotopic composition was measured to be 848‰ (2.3 atom% ^{13}C), and the elemental abundance was 77.9% C, 3.4% H and 14.4% O (Santos et al., 2012). Additional detailed chemical characterization of Ponderosa pine PyOM and precursor wood, including DR-FTIR and solid state NMR, has been reported elsewhere (Chatterjee et al., 2012). Briefly, solid state ^{13}C nuclear magnetic resonance (NMR) and diffuse reflectance Fourier transform infrared spectroscopy (DR-FTIR) of the source pine and PyOM showed with pyrolysis the accumulation of heat resistant aliphatic domains and fused or stacked aromatic rings and diminished polysaccharide-derived oxygenated aliphatic and carboxyl groups (Chatterjee et al., 2012). Aryl or alkene C contributed 93% of the total acquired signal as determined by direct polarization (DP) ^{13}C NMR demonstrating that PyOM used in this study is dominated by aromatic C.

2.2. Artificial weathering of PyOM

Weathering effects were simulated by reacting the fresh, untreated PyOM (PyOMF) in an aqueous slurry for 4 weeks either in the dark (PyOMW), or under UV (254 nm) light (PyOMUV). Briefly, to produce PyOMUV, the original fresh untreated PyOMF (particle size $\leqslant$ 2 mm) was loaded as 30 mg subsamples into 4 separate 16 ml quartz vials (New England Ultraviolet Company, Branford, CT) containing 10 ml of ultra-pure water. The vials were then sealed and attached to a gently rotating carousel (5 rpm) with continuous exposure to two fixed low-pressure mercury lamps, which emit light at 254 nm, for 4 weeks in a procedure modified from Skjemstad et al. (1996). The intensity of incident UV light from these lamps was $\sim 1.5 \times 10^{-9}$ Einstein cm^2/s (Chu et al., 1998; Diehl et al., 2002). Foil-covered vials were also prepared and used as the dark reaction comparisons, simulating only water exposure and leaching. The UV treatment applied to PyOM in this experiment was identical to Chu et al. (1998) and is calculated to produce $\sim$1879 W/cm^2 of energy over the four weeks. This amount of energy is equivalent to $\sim$11 days of solar radiance at mid latitudes (39° 16′ 22 N) at 2944 m above sea level (McKenna and Andreas, 1997).

Prior to isolation of the weathered PyOM, after 4 weeks of treatment, a 3 ml headspace sample was removed from the vials and injected into pre-evacuated exetainer vials (Labco Ltd., Ceredigion, UK) to determine the extent of oxidation of PyOM to CO_2 and to assess the ^{13}C-label content. The contents of the vials were then combined within treatment, filtered to 0.22 μm, using a cellulose acetate filter and air dried to recover the weathered PyOM.

2.3. Analysis of PyOM surface chemistry

2.3.1. Fourier-transform infrared (FTIR)

FTIR spectra of the untreated and weathered PyOM was obtained using a Nicolet 6700 FTIR spectrometer (Thermo Fisher, Waltham, MA). A Smart Diffuse Reflectance accessory (Thermo Fisher, Waltham, MA) was used in the sample bench. The samples were analyzed by mixing 10 mg of PyOM with 190 mg of spectral grade KBr (Pike Technologies, Madison, WI) then grinding in an agate vial for 30 s using a Wig L Bug mixer (Dentsply Rinn, York, PA). The mixtures were then packed into a 6 mm diameter sample cup and the mixture surface was flattened with a metal spatula prior to analysis. DR-FTIR spectra were collected with 64 individual scans which were signal averaged using 4 cm^{-1} optical resolution in the region from 4000 to 580 cm^{-1}. Sample spectra were normalized by a background spectrum of KBr using the standard Kubelka Monk transformation in OMNIC Series Software Version 8.2 (Thermo Fisher, Waltham, MA). Spectra were further analyzed by investigating the peak areas associated with O–H stretching (3600–3300 cm^{-1}), aromatic C–H stretch (3000–3100 cm^{-1}), aliphatic C–H stretch (2850–3000 cm^{-1}), C=O stretch (1700–1725 cm^{-1}), C=O stretching/C=C aromatic stretch (1400–1600 cm^{-1}), and C–O stretch (1210–1320 cm^{-1}) (Cheng et al., 2008; Keiluweit et al., 2010; Demyan et al., 2012). As a semi-quantitative measure, the relative contributions of peak area intensities were calculated as outlined in Demyan et al. (2012) and Harvey et al. (2012). Briefly, a local peak area associated with each functional group was selected by establishing a lower and upper boundary and drawing a local baseline within these boundaries to designate integration limits based on group frequencies reported by Cheng et al. (2008), Keiluweit et al. (2010) and Demyan et al. (2012). The peaks within the established integration limits were then baseline corrected and integrated to obtain peak areas using Grams/32 AI Version 6.0 (Galactic Software, Salem, NH). Ratios of the resultant peak areas were then calculated to determine spectral difference amongst the different types of PyOM. Although FTIR is a bulk analysis, the chemical characteristics and subsequent measured differences with treatment may be attributed to surface chemical phenomenon reported in previous studies (Harvey et al., 2012).

2.3.2. X-ray photoelectron spectroscopy (XPS)

XPS was used to obtain an average surface carbon oxidation assessment of the particles as this method penetrates the top $\sim$10 nm of the surface. For the analysis, 30 mg was sampled from the three initial pools of PyOMF. Approximately 3 mg of PyOM was dusted onto copper tape until the tape was fully covered. Samples were analyzed in a PHI 5600 XPS system using Mg Kα X-rays (1253.6 eV, 15 kV, 300 W) and a high-energy electron energy analyzer, operating at a constant pass energy of 5.85 eV. XP spectra were processed using commercially available software (CasaXPS version 2.3.16, CASA Software, Ltd., Teignmouth, UK) and integration of the relevant peak areas was used for quantification. Each spectrum was given a Shirley background and energy adjusted to 284.6 eV in the C (1s) region.

2.4. Fungal inoculation experiments

To evaluate the response of the white-rot fungus *T. versicolor* (strain MAD-697-R) to untreated and artificially weathered ^{13}C-labeled PyOM, single culture inoculation experiments were established in malt extract agar (MEA), a growth media produced from malted barley with an isotopic composition of −23.8‰ $\delta^{13}C$. The large difference between $\delta^{13}C$ values in the growth media and the PyOM allows for distinction of the two sources in evolved CO_2 and thus is used to determine relative microbial mineralization of source. *T. versicolor* was obtained from the Forest Pathology and Wood Microbiology collection at the University of Minnesota, St. Paul, Minnesota. Decay studies were performed in 12 ml borosilicate exetainer vials (Labco Ltd., Ceredigion, UK) with hard plastic screw cap fitted with glass fiber filter (GF/F) paper to allow for gaseous exchange or septum to permit headspace CO_2 accumulation. PyOM particles were mixed into 0.75 ml of 2% MEA at a loading of 5% of the MEA C. This was poured onto a 1.5 ml, non-nutritive base layer of 3% agar precharged into the vial. The denser base media was included to prevent large PyOM from settling at the bottom of the containers during the incubation period. MEA without PyOM additions was also inoculated and prepared as controls. Microcosms (except for no-fungi controls) were then inoculated with a 1 cm diameter plug taken from the 2% MEA stock plate and incubated for 4 days in the dark at 25 °C without headspace analysis to allow fungal colonization. Headspace monitoring began after day 4 and continued for 36 days. The headspace of each vial was sampled for CO_2 on days 4, 23, 30 and 36 after

1 h accumulation periods. This was done by replacing the GF/F-containing caps with caps fitted with Teflon coated rubber septa, flushing with moistened CO_2 free air prior to accumulation time, and removing 3 ml of headspace from each vial after accumulation of gases. The sample was then injected into pre-evacuated exetainer vials (Labco Ltd., Ceredigion, UK).

2.5. Stable isotope trace gas analysis

To distinguish between growth media or ^{13}C-labeled PyOM in the inoculation experiments, the stable isotope content of evolved CO_2 was determined using a Sercon Cryoprep TG2 interfaced to a Sercon 20-22 Isotope Ratio Mass Spectrometer (IRMS) (Sercon, Crewe, UK). Isotopic ratios are expressed in standard delta notation (δ) and in units of per mil (‰) relative to the Vienna Pee Dee Belemnite (VBDB) standard. The CO_2 carbon source was calculated using a two component mixing model as follows:

$$\delta^{13}C_{measured} = f_{MEA} * \delta^{13}CO_{2MEA} + (1 + f_{MEA}) * \delta^{13}CO_{2MEA+PyOM} \quad (1)$$

$$f_{MEA} + f_{MEA+PyOM=1} \quad (2)$$

Total C respired was calculated using the estimated cumulative C mineralized at each sample time point. This method assumed that the rate of CO_2 evolved for each subsampled time point was representative of the rate of CO_2 evolved during the period of time elapsed since the previous sample point. Cumulative CO_2 was calculated using the following equation:

$$C_i = \sum_{i=1}^{n} R_i \times T_i \quad (3)$$

where C_i is cumulative C mineralized until the current time point (i) of the CO_2 analysis, n is the number of total time points in this experiment, R_i is respiration rate of the current time point, T_i is the time interval between i point and the following time point ($i + 1$). Total C respired was calculated by using the sum of the cumulative CO_2 for all sample points.

2.6. Enzyme activity assays

To determine the oxidative enzyme response of *T. versicolor* to the control and PyOM treatments, a 2,2′-azino-bis-(3-ethylbenzo thiazoline-6-sulfonate) (ABTS) assay was performed on enzymes extracted via micro-centrifugation of growth media, modified from the methods described in Heinonsalo et al. (2012) and Berry et al. (2014). To recover enzymes from the MEA layer, 4 mm square plugs of media plus fungi were extracted from each tube of which replicates within the same treatment were combined and homogenized. Three equal volume subsamples of the homogenate were added to a micro-centrifuge tube with 0.45 µm cellulose acetate membrane filters (Costar Spin-X, Corning Inc., NY) and then centrifuged at room temperature and 15,700*g* for 30 min. Replication, therefore, for the enzyme assays was at the analytical level, not the experimental treatment level.

The reaction solution consisted of 0.5 mM $MnSO_4$, 1.0 mM ABTS, 5 µl of H_2O_2 (added after measuring laccase activity) and 50 mM sodium malonate buffer at pH 6 (Sigma–Aldrich, St. Louis, MO). The supernatant from each micro-centrifuge tube was added (~200 µl) to the reaction solution and the absorbance read at 420 nm after 20 s. After the initial measurement, H_2O_2 was added and absorbance was measured after 20 s. Enzyme activity was quantified against a standard curve prepared by reacting purified laccase of known activity from *T. versicolor* with reaction solution. Peroxidase activity was determined 20 s after the addition of H_2O_2 and was calculated by subtraction of laccase activity from total activity. All activities are reported in mU/ml of supernatant.

2.7. Statistical methods

Each inoculation treatment was prepared in triplicate and standard errors of means for FTIR and stable isotope measurements were calculated from the individual analysis of each replicate. Enzyme assays were done on combined inoculation treatments. Means were compared using a Two-way ANOVA and Tukey's HSD test at $p < 0.05$ using SAS JMP 10 (SAS Institute, Cary, NC).

3. Results

3.1. ^{13}C Isotopic evidence for weathering-induced oxidation of PyOM

Stable isotope analysis of sample headspace after 4 weeks of artificial weathering showed highly ^{13}C-enriched CO_2 values for PyOMUV (~306‰), but only mildly ^{13}C enriched values for PyOMW (~−5.0‰) compared to the head space blank $\delta^{13}C$ CO_2 value (−11‰) (Table 1). The UV weathering-derived CO_2, however, was significantly depleted with respect to the reported $\delta^{13}C$ value of the PyOMF at ~840‰ (Santos et al., 2012). The enriched PyOMUV head space indicates UV promoted oxidation of the PyOM surface, but because the head space and water used in the experiment were not flushed of background CO_2, the stable isotope value was diluted by more than half the anticipated ~840‰ CO_2 value. These values clearly indicate that UV weathering (PyOMUV) resulted in surface oxidation while water leaching (PyOMW) liberated only small amounts of ^{13}C-labeled CO_2.

3.2. Chemical analysis of weathered and fresh PyOM

XPS spectra resolved into %C and %O for each treatment revealed a minor decrease in surface C and a concomitant increase in surface O for the UV light PyOMUV treatment (Table 2). These changes resulted in a slight shift in the elemental O:C ratio from 0.148 (PyOMF) to 0.177 (PyOMUV) indicating a slight increase in surficial oxygen content through photolysis. PYOMW showed minimal change in the XPS analysis.

The FTIR analysis of the PyOM treatments exhibited trends consistent with changes indicated in the XPS analysis. The sum of the combined peak areas of O–H stretching vibrations associated with free hydroxyl groups (3630, 3535 and 3490 cm^{-1}) decreased for both PyOMUV and PyOMW with respect to PyOMF, with the largest decrease observed in the UV light treatment (Fig. 1a and Table 3). This change was driven primarily by 3630 cm^{-1} as there was no significant change in peak intensity at this wavelength among the treatments (Fig. 1). The aromatic C–H and C=C stretching vibrations (3050 cm^{-1} and 1600 cm^{-1}) decreased in PyOMUV with respect to PyOMF (Fig. 1b and c) while only the C=C stretching vibration (1600 cm^{-1}) decreased in PyOMW (Fig. 1b and c). For PyOMUV, the aliphatic C–H (2965, 2910 and 2870 cm^{-1}) and the carbonyl C=O (1705 cm^{-1}) stretching vibrations increased relative to PyOMF and PyOMW (Fig. 1b and c). This same region decreased in PyOMW relative to PyOMF. The region from 1274 cm^{-1} (C–O stretching vibration and OH plane deformation) exhibited a

Table 1
Mean $\delta^{13}C$ (‰) values of headspace CO_2 with standard errors ($n = 5$) after four weeks of artificial weathering in a water slurry in sealed quartz vials while exposed to UV-light (PyOMUV) and in the dark (PyOMW).

Treatment	CO_2 (µmole)	$\delta^{13}C$ (‰)
PyOMF[a]	– ± –	840 ± 0.20
PyOMW	0.13 ± 0.01	−5.81 ± 3.68
PyOMUV	1.36 ± 0.10	305.7 ± 16.0

[a] This value was obtained from elemental analysis of untreated PyOM (Santos et al., 2012).

Table 2
X-ray photoelectron spectroscopy (XPS) analysis resolved into C and O elemental % for fresh pyrogenic organic matter (PyOMF) and artificially weathered forms of PyOM treated for four weeks in a water slurry either exposed to UV light (PyOMUV) or in the dark (PyOMW). Measurements were made prior to addition to fungal inoculation experiments.

Element	PyOMF	PyOMW	PyOMUV
%C	85.6	84.8	83.2
%O	12.7	12.8	14.7

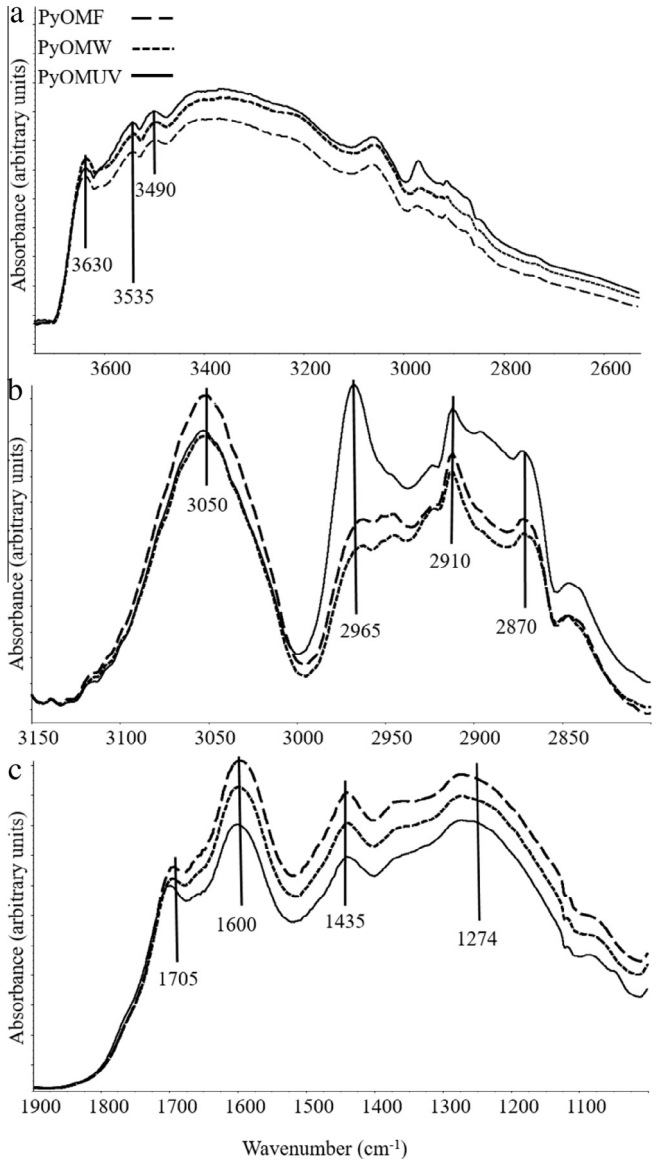

Fig. 1. FTIR spectra of fresh pyrogenic organic matter (PyOMF) and artificially weathered forms treated for four weeks in a water slurry either exposed to UV light (PyOMUV) or in the dark (PyOMW) in the: (a) O–H stretching region (3600–3300 cm^{-1}), (b) C–H stretching region (3100–2820 cm^{-1}), and (c) the lower frequency fingerprint region (1710–1200 cm^{-1}).

decrease for both weathering treatments, but with the PyOMUV treatment exhibiting a large (ca. 50%), reduction relative to the initial PyOMF.

The relative changes of functional groups attributed to oxidized carbon (carbonyl, carboxylate), aliphatic carbon (C–H), aromatic C=C and C=C–H, and OH stretching vibrations (those highly susceptible to photochemical oxidation) are used herein to elucidate

Table 3
FTIR band assignments and peak area for fresh pyrogenic organic matter (PyOMF) and artificially weathered forms of PyOM treated for four weeks in a water slurry either exposed to UV light (PyOMUV) or in the dark (PyOMW). Measurements were made prior to addition to fungal inoculation experiments. The mean and standard error ($n = 3$) of each of the PyOMF, PyOMW, and PyOMUV treatments is shown.

Wavenumber (cm^{-1})	Assignment	PyOMF area	PyOMW area	PyOMUV area
3630, 3535, 3490	Free O–H stretching vibration	4.5 ± 0.9	3.7 ± 0.3	3.3 ± 0.3
3050	Aromatic C–H stretching vibration	1.4 ± 0.3	1.1 ± 0.1	1.6 ± 0.2
2965, 2910, 2870	Aliphatic C–H stretching vibration	1.3 ± 0.1	1.1 ± 0.0	2.2 ± 0.3
1705	Carbonyl stretching vibration of carboxylic groups	3.2 ± 0.2	2.8 ± 0.2	5.0 ± 0.9
1600	Aromatic C=C vibration, C=O stretching vibration	14.7 ± 0.9	11.7 ± 0.8	9.1 ± 0.9
1435	Aromatic skeletal vibration with C–H in plane deformation or C–O stretching vibration from carbonates	8.0 ± 0.4	6.2 ± 0.9	5.2 ± 0.4
1274	C–O stretching vibration, OH plane deformation	37 ± 4	30 ± 7	20 ± 3

Table 4
Ratios of FTIR peak areas for of aryl C–H stretching vibration to aliphatic C–H stretching vibration (3050/(2965, 2910, 2870 cm^{-1})), carbonyl C=O stretching vibration to aryl C=C vibration (1705/1600 cm^{-1}), C–O stretching to OH stretching ((1274/3630, 3535, 3490) cm^{-1}), carbonyl to carboxylate (1705/1435 cm^{-1}), and aryl C=C stretching vibration to aliphatic C–H stretching vibration (1600/2965, 2910, 2870 cm^{-1}) for PyOMF, PyOMW, and PyOMUV treatments. The mean and standard error ($n = 3$) of each of the PyOMF, PyOMW, and PyOMUV treatments is shown. Measurements were made prior to addition to fungal inoculation experiments.

Band assignments	Ratio of wavenumbers (cm^{-1})	PyOMF ratio values	PyOMW ratio values	PyOMUV ratio values
Carbonyl C=O/Ar C=C	1705/1600	0.2 ± 0.0	0.3 ± 0.0	0.6 ± 0.1
C–O/OH	1274/3630, 3535, 3490	8.5 ± 0.7	8 ± 1	6.2 ± 0.9
Carbonyl C=O/ Carboxylate C–O	1705/1435	0.4 ± 0.0	0.50 ± 0.0	1.0 ± 0.1
Ar C–H/AL–CH	3050/2965, 2910, 2870	1.1 ± 0.1	1.0 ± 0.0	0.7 ± 0.0
Ar C=C /AL C–H	1600/2965, 2910, 2870	11.6 ± 0.9	10.2 ± 0.3	4.1 ± 0.5

how artificial weathering changes surface chemical properties that could influence interactions with fungi (Table 4). The ratios of carbonyl C=O stretching vibration (1705 cm^{-1}) to aryl C=C vibration (1600 cm^{-1}) versus aryl C–H stretching vibration (3050 cm^{-1}) to aliphatic C–H stretching vibration (2965, 2910 and 2870 cm^{-1}) shows that the PyOMUV samples become relatively enriched in oxidized carbonyl-C (C=O) over aryl-C while simultaneously trending toward a chemistry relatively enriched in aliphatic C at the expense of aromatic C–H (Table 4). Additionally, the relative contribution of the carbonyl (1705 cm^{-1}) to carboxylate (1435 cm^{-1}) C–O band increased significantly in the PyOMUV samples compared to both PyOMF and PyOMW (Table 4). Relative changes of the C–O to broad OH stretching vibrations (Table 4) exhibit a dramatic reduction concomitant with the shift to aliphatic carbon driven by a large loss in the C–O stretch associated with aromatic hydroxyl groups. Together, these results reflect the combined effects of photo-oxidation and water leaching of soluble carboxylic groups.

3.3. Total carbon respired and carbon source partitioning

Over the 36 day incubation with *T. versicolor* the cumulative production of CO_2 ranged from a low of 16.6 mg C/g MEA C for the MEA + PyOMF treatment to a high of 260 mg C/g MEA C for the MEA + PyOMW treatment (Fig. 2). The addition of PyOMF to MEA resulted in a marginally significant ($\alpha = 0.10$) reduction in CO_2 efflux with respect to the MEA-fungi control. Addition of both weathered PyOM treatments increased the production of CO_2 by over 2× for PyOMUV and 5× for PyOMW, respectively.

Across all four treatments, the average $\delta^{13}C$ values of respired CO_2 ranged from −23.5 (±0.8), −22.1 (±1.1), −23.9 (±0.5), and −24.5 (±1.5) for the 4, 23, 30 and 36 day samplings, respectively. Despite the large differences in the concentration in CO_2 efflux among the treatments, the $\delta^{13}C$ values of the CO_2 showed no difference among the treatments or between the weathered and control experiments.

3.4. Enzyme activity

Laccase activity ranged from 50.8 (control) to 265.8 mU/ml media (PyOMW) while peroxidase ranged from 55.3 (control) to 386.4 mU/ml media (PyOMW) (Fig. 3). The addition of PyOMUV and PyOMW resulted in a significant increase in both laccase and peroxidase activities above the MEA-fungi control ($\alpha = 0.05$) which had the lowest values of both enzymes. The addition of PyOMF resulted in only a moderate increase ($\alpha = 0.10$) in laccase and no increase in peroxidase activity. As with total C respired, the addition of PyOMW resulted in the most significant effects on enzyme activity.

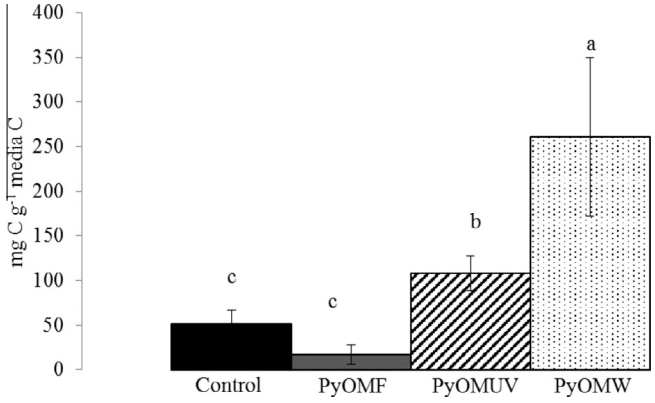

Fig. 2. Total C respired, normalized per gram of malt media agar (MEA) C, over 36 days for un-amended MEA (control) and MEA amended with fresh pyrogenic organic matter (PyOMF) and artificially weathered forms treated for four weeks in a water slurry either exposed to UV light (PyOMUV) or in the dark (PyOMW). Treatments that do not share the same letters are significantly different from each other ($\alpha = 0.05$).

4. Discussion

4.1. UV-treatment induced PyOM surface oxidation consistent with natural weathering

Weathering by UV exposure and water leaching induced significant changes to the surface chemistry of PyOM particles (PyOMUV) used in this incubation (Table 4). Overall, these chemical changes are consistent with expected surface alteration of highly condensed aromatic carbon substances by photo-oxidation (Chen and Jafvert, 2010; Bitter et al., 2014). Aromatic carbon readily absorbs UV light, and in the presence of oxygen and water leads to the oxidation and cleavage of the C=C bonds resulting in the formation of hydroxyl, carbonyl, and/or carboxylic groups (Bertilsson and Stefan, 1998; Wu et al., 2001). Observed changes in our current study included increased surface O content (Table 2) and a general increase in carbonyl and aliphatic chemical groups at the expense of aromatic ones (Table 3). The changes in FTIR signatures for the leached weathering treatment (PyOMW) (Fig. 1 and Tables 3 and 4), which were limited to minor decreases in aromatic (3050 and 1600 cm^{-1}), minor increases in carboxyl stretches (1435 cm^{-1}), and a decrease in the broad hydroxyl distribution (3630, 3535 and 3490 cm^{-1}) may be attributed to redistribution of more mobile moieties from within the PyOM structure to the surface without significant oxidation. These chemical alterations are also consistent with other investigations of artificial and natural aging of PyOM, which showed an increase in surficial carbonyl and carboxylic acid functional groups (Yao et al., 2010; LeCroy et al., 2013; Liu et al., 2013).

Chemical weathering of PyOM also involves a decrease in the degree of condensation of the aromatic ring structure. Weathered PyOM that has undergone extensive surface oxidation were shown to consist of less than ten fused aromatic rings substituted with carboxyl groups and one or two hydroxyl groups compared to greater than ten for their un-weathered precursors (Mao et al., 2012). In our study, the higher intensity of both aliphatic and aryl C–H peak areas in PyOMUV is likely the result of a number additive processes including the leaching and photochemical decarboxylation of carboxylic groups, the reabsorption of aliphatic compounds mobilized from the interior of the PyOM particles, and the photochemical breaking of the aryl C=C bonds (Cheng et al., 2006).

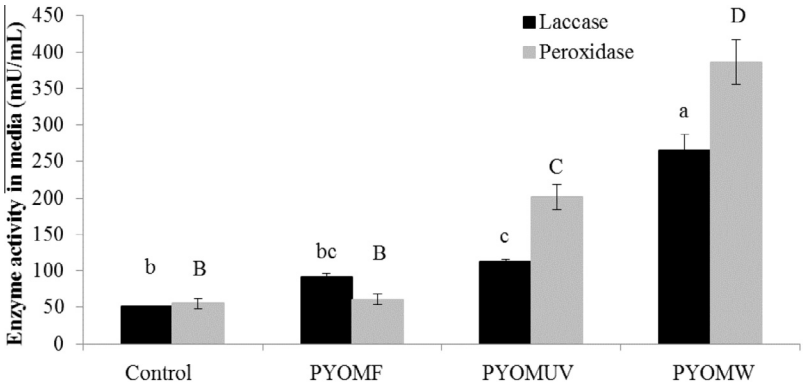

Fig. 3. Laccase and peroxidase enzyme activity from *T. versicolor* inoculated microcosms ($n = 3$) of malt extract agar (MEA) (control) and MEA containing either fresh pyrogenic organic matter (PyOMF) or artificially weathered forms treated for four weeks in a water slurry either exposed to UV light (PyOMUV) or in the dark (PyOMW). Treatments which do not share letters are significantly different for laccase (lower case) and peroxidase (upper case) activity ($\alpha = 0.05$).

While most chemical characterization studies of PyOM aging in soils have involved the recovery of 6 month to 100 year PyOM, short-term exposure of PyOM in soils where microbial interactions may be the dominant control on chemical change have also resulted in increased surface O and carboxyl groups (Hockaday et al., 2007; Nguyen et al., 2009; LeCroy et al., 2013) as we have also seen here. Surficial changes in soil aging, however, have an added ambiguity in that it is nearly impossible to distinguish microbial oxidation from sorption of oxidized dissolved organic matter in the soil.

4.2. Artificial weathering of PyOM induces fungal enzymatic response

We found a significant increase in both laccase and peroxidase enzyme activities with the addition of PyOMUV and PyOMW ($\alpha = 0.05$). However, PyOMF resulted in only a marginal increase in laccase activity ($\alpha = 0.10$) compared to the no-PyOM control (Fig. 3). In contrast to our original hypothesis, PyOMW exhibited a significantly greater response in enzyme activity than PyOMUV ($p < 0.001$). These findings, in conjunction with the chemical characterization data, demonstrate that surface PyOM chemistry and degree of condensation play significant roles in microbial response to PyOM (D'Annibale et al., 2005; Schreiner et al., 2009; Arun and Eyini, 2011; Berry et al., 2014).

The distinct chemical differences observed for PyOMF, PyOMUV and PyOMW (Fig. 1 and Tables 3 and 4) should influence a variety of physical properties such as inorganic and organic sorptive and binding capacity, and surface charge, which could be a controlling factor in the distinct enzymatic and mineralization responses observed (Kasozi et al., 2010; Lehmann et al., 2011). These chemical differences may even influence the binding and thus the activity of extracellular enzymes. Cho and Bailey (1978) observed decreased apparent glucose oxidase and gluconolactonase activities with the addition of char-based activated carbon to a maltose solution inoculated with the enzymes. Similarly, a study by Zhang and Yu (2000) demonstrated that activated C decreased dye decolorization and laccase activity when added to an azo dye inoculated with *T. versicolor*. In the context of the present study, such findings indicate that our untreated PyOMF may have inhibited the enzymatic activity of *T. versicolor* explaining the marginal suppression of MEA C mineralization.

In general, our results for PyOMUV and PyOMW in comparison to PyOMF are consistent with previous work on the white-rot fungal response to single wall carbon nanotubes (CNTs), highly condensed aromatic carbon structures with different degrees of surface oxidation (Berry et al., 2014). These authors found that the two white rot fungi *T. versicolor* and *Phlebia tremellosa* both increased the activity of laccase and peroxidase enzymes in single culture media when CNT, with just 3% carboxyl content, were added to the growth media. However, these same fungi exhibited no response when pure, unfunctionalized CNT were added, leading to the hypothesis that surface carboxyl functional groups caused an increase in degradative enzyme activity and thus oxidative aging would be a critical factor for environmental microbial degradation. This response may be governed by the sorptive capacity of PyOM and other HCAC (Kasozi et al., 2010; Masiello et al., 2013). In some cases, this could lead to the disruption of extracellular signaling of the fungus, as demonstrated by Masiello et al. (2013) who observed reduced gene expression by gram negative bacteria as a result of sorption of stimulatory compounds on the surface of PyOM. This has implications for the weathered (leached and photo-treated) analogs of PyOMF as increased weathering may lower capacity to bind key regulatory compounds. These results suggest that substrate and enzyme sorption, occlusion of enzyme active sites, and binding of regulatory compounds may be involved in the inhibition of substrate mineralization in PyOMF and to a lesser degree weathered PyOM. The overall suppressive effect of PyOMF is in keeping with strong adsorption of both extracellular enzymes and nutrients which should limit decomposition of both media and PyOM; similar to the interpretation of past mesocosm studies where activated char was shown to bind enzyme active sites and prevented dye decolorization (Zhang and Yu, 2000).

It is not immediately clear, however, what mechanisms would result in the seemingly non-linear relationship between surface chemical change, highest for PyOMUV, and fungal reactivity response, highest for PyOMW. Our original hypothesis stated that, although this particular 450 °C PyOM has been shown to have very low lability in soil (Santos et al., 2012), the oxidized PyOMUV would exhibit the highest fungal enzyme activity, PyOM decomposition, and MEA decomposition as this material would leach lignin-like signaling compounds, like veratryl alcohol (Dekker et al., 2001), to induce oxidative enzyme production (Schreiner et al., 2009; Berry et al., 2014). Interestingly, although PyOMW exhibited surface chemical changes far less than PyOMUV, as exhibited by the XPS, FTIR, and $^{13}CO_2$ analyses (Tables 1–3 and Fig. 1), it induced the greatest enzyme response and MEA priming. Taken together, the relative response between PyOMF and PyOMUV can be reasonably explained by suppressive surface binding effects of PyOMF and an amplifying reactivity effect from PyOMUV because of potential inducer compounds; a hypothesis consistent with earlier studies (Berry et al., 2014). That explanation, unfortunately, runs counter to the relative reactivity observed between PyOMUV and PyOMW and their assumed chemical differences. One possible explanation that could make sense of the three treatment responses might be gathered from the FTIR data. The increase in aryl CH and aliphatic CH stretching vibrations in PyOMUV relative to PyOMF (Fig. 1 and Tables 3 and 4) suggests that the PyOMUV surface may be relatively more hydrophobic than PyOMW and thus could have potentially greater surface sorptive properties for enzymes or labile MEA compounds. Without further chemical characterization, it is not possible to unequivocally determine relative controls.

4.3. Weathered PyOM induces fungal priming but is not simultaneously degraded

Similar to the differential response of the enzyme activity upon addition of fresh and weathered PyOM, *T. versicolor* exhibited a distinct capacity to mineralize the MEA growth media C based on PyOM type (Fig. 2). We anticipated that total C mineralized would increase with degree of simulated weathering in the order MEA < PyOMF < PyOMW < PyOMUV, and that each PyOM treatment would induce some degree of MEA decomposition. However, the greatest yield in respired CO_2 was in the PyOMW treatment with the overall relative rank as PyOMF $\leqslant$ MEA < PyOMUV < PyOMW. In fact, PyOMF mildly suppressed ($\alpha = 0.1$) MEA mineralization with respect to the no-PyOM MEA-fungi control. Surprisingly, and contrary to our hypotheses, there was no PyOM $^{13}CO_2$ mineralized during the incubation process, at least after the first week of the experiment when CO_2 accumulation began. Therefore, the main effect of the weathered PyOM was to induce, or positively prime (Kuzyakov et al., 2009) MEA decomposition while the main influence of the PyOMF was to mildly suppress (or negatively prime) MEA decomposition. Certainly, under the appropriate conditions, *T. versicolor*, and many white-rot fungi in general, have the capacity to mineralize highly condensed polyaromatic carbon materials, which has been shown in similar laboratory and soil inoculations (Zhang and Yu, 2000; Schreiner et al., 2009; Arun and Eyini, 2011). Fungal decay studies using *T. versicolor* and highly condensed aromatic compounds have also shown that carbon mineralization potential decreases with the degree of ring condensation (Andersson et al., 2003; Atagana, 2009).

Andersson et al. (2003) also observed a suppression of PAH degradation after wood addition. With respect to large, highly condensed aromatic particles like PyOM, prior field and laboratory soil mesocosm studies, including one by Santos et al. (2012) that investigated the exact PyOMF materials used in the present study, demonstrated PyOM oxidation to CO_2 and incorporation into both fungal and bacterial PLFAs (Maestrini et al., 2014a). Furthermore, Santos et al. (2012) showed that uptake of PyOM C into fungal PLFA was lower (>20 mol%) than in bacterial PLFA while the reverse was observed for soil-derived C. A low preference for PyOM by fungi is in agreement with the results demonstrated herein that showed no PyOM-^{13}C in the headspace and indicates either a preference for MEA C, relatively lower substrate use efficiency, the inability of fungi to penetrate PyOM pore spaces to access labile PyOM C, or the need for complex microbial consortia (Boonchan et al., 2000; Jin et al., 2010; Zimmerman et al., 2011).

A portion of the resilience of PyOM in soil has been ascribed, in part, to enhancement of physical protection mechanisms within soil aggregates (Hamer et al., 2004; Zimmerman et al., 2011) or coating by a protective rind (Brodowski et al., 2006). Kasozi et al. (2010) showed that compounds containing hydroxyl and carboxyl groups can be progressively sorbed to PyOM surfaces over time and that PyOM can sorb up to 0.1% of its weight in natural organic matter (NOM) and about 1% of low molecular weight phenolic compounds. While soil aggregation is not possible in the present study, it suggests that there is potential for PyOM suspended in a nutrient rich growth media, to be protected from mineralization by essentially being coated in a protective layer that provides a barrier between the PyOM surface and extracellular enzymes.

Previous PyOM-soil mesocosm studies exhibit a positive priming effect at the early stage of the incubation (Hamer et al., 2004; Zimmerman, 2010; Zimmerman et al., 2011; Jones et al., 2011; Cross and Sohi, 2011). Proposed mechanisms for this phenomenon include co-metabolism through extracellular enzyme production, microbial community behavior, i.e., copiotrophs versus oligotrophs, and sorption of carbon sources to PyOM (Hamer et al., 2004; Zimmerman et al., 2011; Maestrini et al., 2014a). However, our study shows that no PyOM C was mineralized as CO_2, suggesting that these labile components are either inaccessible to fungi, or play a different role in the mineralization process when abundant metabolizable carbon is present. It is important to note that we allowed the fungi to incubate with the media and PyOM while the hyphae initially grew before sampling the headspace. It is possible that all the rapidly metabolizable PyOM C was consumed in this short time frame. While our study focused on one species of fungi, these results suggest possibly a less-significant role of fungi in PyOM decomposition; a finding consistent with recently published studies from soil-PyOM incubations. Using ^{13}C-labeled PyOM to trace metabolic uptake into phospholipid fatty acids both Santos et al. (2012) and Farrell et al. (2013) demonstrated that gram positive bacteria were able to incorporate more PyOM C in their cells than either gram negative bacteria or fungi and they also showed that fungi had a greater preference for wood. It is also possible that if our experiments used PyOM produced over range of production temperature we would observe very different results with respect to fungal accessibility of the weathered and fresh PyOM as has been demonstrated with soil incubations (Luo et al., 2011; Zimmerman et al., 2011).

5. Conclusions

This study provides the first evidence for the direct role of surface oxidation in the response of white-rot fungi to pyrogenic organic matter in a decomposition study. Addition of weathered PyOM resulted in increased mineralization of malt extract media as indicated by increases in both CO_2 evolved and enzyme activity, serving as a microbial inducer rather than an available C source. While this study focused on one species of fungi, these results may shed light on the role of fungi in PyOM studies involving soil and sediments and help to explain why microbial priming results vary extensively among experiments. It could be that fungi are more involved in the positive priming of SOC in the presence of PyOM than bacteria. While this study did not measure the sorptive character of the different PyOM used, our results demonstrate that over time, weathering of PyOM might aid in the sequestration of C by increased binding of organic compounds with increased weathering by altering surface charge. However, further study is needed to confirm that sorption to PyOM surface is a major factor in the response of enzymatic activity and total C mineralized as well as confirming whether these fungi exhibit strategies that select for SOC over PyOM in priming studies. The increased enzymatic and positive priming response of *T. versicolor* to weathered PyOM highlights the importance of weathering-induced chemistry in controlling PyOM–microbe–soil carbon interactions.

Acknowledgments

The authors would like to thank the reviewers for their comments and suggestions, which were invaluable while completing this manuscript. The authors also acknowledge support from the United States National Science Foundation award BIO-1127253. The award was co-funded by the Divisions of Environmental Biology and Earth Sciences. The authors also thank Dr. Howard Fairbrother, The Johns Hopkins University, for assistance with XPS analysis and characterization of PyOM materials used in this study, Dr. Gnanasiri S. Premachandra, Purdue University, for assistance with DR-FTIR analysis of PyOM, and Dr. Robert Blanchette, University of Minnesota, for providing fungal cultures.

Appendix A. Supplementary data

Supplementary data associated with this article can be found, in the online version, at http://dx.doi.org/10.1016/j.orggeochem.2015.12.003.

Associate Editor—**Myrna Simpson**

References

Adams, M.A., 2013. Mega-fires, tipping points and ecosystem services: managing forests and woodlands in an uncertain future. Forest Ecology and Management 294, 250–261.

Andersson, B.E., Lundstedt, S., Tornberg, K., Schnürer, Y., Öberg, L.G., Mattiasson, B., 2003. Incomplete degradation of polycyclic aromatic hydrocarbons in soil inoculated with wood-rotting fungi and their effect on the indigenous soil bacteria. Environmental Toxicology and Chemistry 22, 1238–1243.

Arun, A., Eyini, M., 2011. Comparative studies on lignin and polycyclic aromatic hydrocarbons degradation by basidiomycetes fungi. Bioresource Technology 102, 8063–8070.

Atagana, H.I., 2009. Biodegradation of PAHs by fungi in contaminated-soil containing cadmium and nickel ions. African Journal of Biotechnology 8, 5780–5789.

Bell, M.J., Worrall, F., 2011. Charcoal addition to soils in NE England: a carbon sink with environmental co-benefits? Science of the Total Environment 409, 1704–1714.

Berry, T.D., Filley, T.R., Blanchette, R.A., 2014. Oxidative enzymatic response of white-rot fungi to single-walled carbon nanotubes. Environmental Pollution 193, 197–204.

Bertilsson, S., Stefan, L.J., 1998. Photochemically produced carboxylic acids as substrates for freshwater bacterioplankton. Limnology and Oceanography 43, 885–895.

Bird, J.A., Torn, M.S., 2006. Fine roots vs. needles: a comparison of ^{13}C and ^{15}N dynamics in a ponderosa pine forest soil. Biogeochemistry 79, 361–382.

Bitter, J.L., Yang, J., Milani, S.B., Jafvert, C.T., Fairbrother, D.H., 2014. Transformations of oxidized multiwalled carbon nanotubes exposed to UVC, 254 nm irradiation. Environmental Science: Nano 1, 324–337.

Bond, T.C., Doherty, S.J., Fahey, D.W., Forster, P.M., Berntsen, T., DeAngelo, B.J., Flanner, M.G., Ghan, S., Kärcher, B., Koch, D., 2013. Bounding the role of black carbon in the climate system: a scientific assessment. Journal of Geophysical Research: Atmospheres 118, 5380–5552.

Boonchan, S., Britz, M.L., Stanley, G.A., 2000. Degradation and mineralization of high-molecular-weight polycyclic aromatic hydrocarbons by defined fungal–bacterial cocultures. Applied and Environmental Microbiology 66, 1007–1019.

Brodowski, S., John, B., Flessa, H., Amelung, W., 2006. Aggregate-occluded black carbon in soil. European Journal of Soil Science 57, 539–546.

Chatterjee, S., Santos, F., Abiven, S., Itin, B., Stark, R., Bird, J., 2012. Elucidating the chemical structure of pyrogenic organic matter by combining magnetic resonance, mid-infrared spectroscopy and mass spectrometry. Organic Geochemistry 51, 35–44.

Chen, C.Y., Jafvert, C.T., 2010. Photoreactivity of carboxylated single-walled carbon nanotubes in sunlight: reactive oxygen species production in water. Environmental Science and Technology 44, 6674–6679.

Cheng, C.H., Lehmann, J., 2009. Ageing of black carbon along a temperature gradient. Chemosphere 75, 1021–1027.

Cheng, C.H., Lehmann, J., Thies, J.E., Burton, S.D., Engelhard, M.H., 2006. Oxidation of black carbon by biotic and abiotic processes. Organic Geochemistry 37, 1477–1488.

Cheng, C.H., Lehmann, J., Engelhard, M.H., 2008. Natural oxidation of black carbon in soils: Changes in molecular form and surface charge along a climosequence. Geochimica et Cosmochimica Acta 72, 1598–1610.

Cho, Y.K., Bailey, J.E., 1978. Immobilization of enzymes on activated carbon: properties of immobilized glucoamylase, glucose oxidase, and gluconolactonase. Biotechnology and Bioengineering 20, 1651–1665.

Chu, W., Jafvert, C.T., Diehl, C.A., Marley, K., Larson, R.A., 1998. Phototransformations of polychlorobiphenyls in Brij 58 micellar solutions. Environmental Science and Technology 32, 1989–1993.

Clarke, A.D., Noone, K.J., 1985. Soot in the Arctic snowpack: a cause for perturbations in radiative transfer. Atmospheric Environment 19, 2045–2053.

Cohen-Ofri, I., Weiner, L., Boaretto, E., Mintz, G., Weiner, S., 2006. Modern and fossil charcoal: aspects of structure and diagenesis. Journal of Archaeological Science 33, 428–439.

Cross, A., Sohi, S.P., 2011. The priming potential of biochar products in relation to labile carbon contents and soil organic matter status. Soil Biology and Biochemistry 43, 2127–2134.

D'Annibale, A., Ricci, M., Leonardi, V., Quaratino, D., Mincione, E., Petruccioli, M., 2005. Degradation of aromatic hydrocarbons by white-rot fungi in a historically contaminated soil. Biotechnology and Bioengineering 90, 723–731.

Dekker, R.F.H., Vasconcelos, A.F.D., Barbosa, A.M., Giese, E.C., Paccola-Meirelles, L., 2001. A new role for veratryl alcohol: regulation of synthesis of lignocellulose-degrading enzymes in the ligninolytic ascomyceteous fungus, *Botryosphaeria* sp.; influence of carbon source. Biotechnology Letters 23, 1987–1993.

Demyan, M.S., Rasche, F., Schulz, E., Breulmann, M., Müller, T., Cadisch, G., 2012. Use of specific peaks obtained by diffuse reflectance Fourier transform mid-infrared spectroscopy to study the composition of organic matter in a Haplic Chernozem. European Journal of Soil Science 63, 189–199.

Diehl, C.A., Jafvert, C.T., Marley, K.A., Larson, R.A., 2002. Surfactant-assisted UV-photolysis of nitroarenes. Chemosphere 46, 553–560.

Environmental Protection Agency, 2012. Report to Congress on Black Carbon. EPA Publication 450/R-12-001.

Farrell, M., Kuhn, T.K., Macdonald, L.M., Maddern, T.M., Murphy, D.V., Hall, P.A., Singh, B., Baumann, K., Krull, E.S., Baldock, J.A., 2013. Microbial utilisation of biochar-derived carbon. Science of the Total Environment 465, 288–297.

Fujii, K., Uemura, M., Hayakawa, C., Funakawa, S., Kosaki, T., Ohta, S., 2009. Fluxes of dissolved organic carbon in two tropical forest ecosystems of East Kalimantan, Indonesia. Geoderma 152, 127–136.

Glaser, B., Haumaier, L., Guggenberger, G., Zech, W., 1998. Black carbon in soils: the use of benzenecarboxylic acids as specific markers. Organic Geochemistry 29, 811–819.

Gomez, J.D., Denef, K., Stewart, C.E., Zheng, J., Cotrufo, M.F., 2014. Biochar addition rate influences soil microbial abundance and activity in temperate soils. European Journal of Soil Science 65, 28–39.

Hamer, U., Marschner, B., Brodowski, S., Amelung, W., 2004. Interactive priming of black carbon and glucose mineralisation. Organic Geochemistry 35, 823–830.

Hamilton, G.A., Hartnett, H.E., 2013. Soot black carbon concentration and isotopic composition in soils from an arid urban ecosystem. Organic Geochemistry 59, 87–94.

Hammes, K., Schmidt, M.W.I., 2009. Changes of biochar in soil. In: Lehmann, J., Joseph, S. (Eds.), Biochar for Environmental Management: Science and Technology. Earth Scan, London, pp. 169–182.

Hammes, K., Smernik, R.J., Skjemstad, J.O., Schmidt, M.W., 2008. Characterisation and evaluation of reference materials for black carbon analysis using elemental composition, colour, BET surface area and ^{13} C NMR spectroscopy. Applied Geochemistry 23, 2113–2122.

Hart, S., Luckai, N., 2013. Review: charcoal function and management in boreal ecosystems. Journal of Applied Ecology 50, 1197–1206.

Harvey, O.R., Herbert, B.E., Kuo, L.J., Louchouarn, P., 2012. Generalized two-dimensional perturbation correlation infrared spectroscopy reveals mechanisms for the development of surface charge and recalcitrance in plant-derived biochars. Environmental Science and Technology 46, 10641–10650.

Heinonsalo, J., Kabiersch, G., Niemi, R.M., Simpanen, S., 2012. Filter centrifugation as a sampling method for miniaturization of extracellular fungal enzyme activity measurements in solid media. Fungal Ecology 5, 261–269.

Hockaday, W.C., Grannas, A.M., Kim, S., Hatcher, P.G., 2006. Direct molecular evidence for the degradation and mobility of black carbon in soils from ultrahigh-resolution mass spectral analysis of dissolved organic matter from a fire-impacted forest soil. Organic Geochemistry 37, 501–510.

Hockaday, W.C., Grannas, A.M., Kim, S., Hatcher, P.G., 2007. The transformation and mobility of charcoal in a fire-impacted watershed. Geochimica et Cosmochimica Acta 71, 3432–3445.

Hofrichter, M., Vares, T., Kalsi, M., Galkin, S., Scheibner, K., Fritsche, W., Hatakka, A., 1999. Production of manganese peroxidase and organic acids and mineralization of ^{14}C-labelled lignin (^{14}C-DHP) during solid-state fermentation of wheat straw with the white rot fungus *Nematoloma frowardii*. Applied and Environmental Microbiology 65, 1864–1870.

Jin, H., Heller, D.A., Kalbacova, M., Kim, J.H., Zhang, J., Boghossian, A.A., Maheshri, N., Strano, M.S., 2010. Detection of single-molecule H_2O_2 signalling from epidermal growth factor receptor using fluorescent single-walled carbon nanotubes. Nature Nanotechnology 5, 302–309.

Jones, D.L., Murphy, D.V., Khalid, M., Ahmad, W., Edwards-Jones, G., DeLuca, T.H., 2011. Short-term biochar-induced increase in soil CO_2 release is both biotically and abiotically mediated. Soil Biology and Biochemistry 43, 1723–1731.

Kasozi, G.N., Zimmerman, A.R., Nkedi-Kizza, P., Gao, B., 2010. Catechol and humic acid sorption onto a range of laboratory-produced black carbons (biochars). Environmental Science and Technology 44, 6189–6195.

Kauffman, N., Dumortier, J., Hayes, D.J., Brown, R.C., Laird, D.A., 2014. Producing energy while sequestering carbon? The relationship between biochar and agricultural productivity. Biomass and Bioenergy 63, 167–176.

Kawamoto, K., Ishimaru, K., Imamura, Y., 2005. Reactivity of wood charcoal with ozone. Journal of Wood Science 51, 66–72.

Keiluweit, M., Nico, P.S., Johnson, M.G., Kleber, M., 2010. Dynamic molecular structure of plant biomass-derived black carbon (biochar). Environmental Science and Technology 44, 1247–1253.

Keith, A., Singh, B., Singh, B.P., 2011. Interactive priming of biochar and labile organic matter mineralization in a smectite-rich soil. Environmental Science and Technology 45, 9611–9618.

Khalizov, A.F., Xue, H., Wang, L., Zheng, J., Zhang, R., 2009. Enhanced light absorption and scattering by carbon soot aerosol internally mixed with sulfuric acid. The Journal of Physical Chemistry 113, 1066–1074.

Kuhlbusch, T.A., 1998. Enhanced: black carbon and the carbon cycle. Science 280, 1903–1904.

Kuzyakov, Y., Subbotina, I., Chen, H., Bogomolova, I., Xu, X., 2009. Black carbon decomposition and incorporation into soil microbial biomass estimated by ^{14}C labeling. Soil Biology and Biochemistry 41, 210–219.

Laird, D.A., Fleming, P., Davis, D.D., Horton, R., Wang, B., Karlen, D.L., 2010a. Impact of biochar amendments on the quality of a typical Midwestern agricultural soil. Geoderma 158, 443–449.

Laird, D., Fleming, P., Wang, B., Horton, R., Karlen, D., 2010b. Biochar impact on nutrient leaching from a Midwestern agricultural soil. Geoderma 158, 436–442.

LeCroy, C., Masiello, C.A., Rudgers, J.A., Hockaday, W.C., Silberg, J.J., 2013. Nitrogen, biochar, and mycorrhizae: alteration of the symbiosis and oxidation of the char surface. Soil Biology and Biochemistry 58, 248–254.

Lehmann, J., Gaunt, J., Rondon, M., 2006. Bio-char sequestration in terrestrial ecosystems – a review. Mitigation and Adaptation Strategies for Global Change 11, 395–419.

Lehmann, J., Czimczik, C., Laird, D., Sohi, S., 2009. Stability of biochar in soil. In: Lehmann, J., Joseph, S. (Eds.), Biochar for Environmental Management: Science and Technology. Earth Scan, London, pp. 183–206.

Lehmann, J., Rillig, M.C., Thies, J., Masiello, C.A., Hockaday, W.C., Crowley, D., 2011. Biochar effects on soil biota – a review. Soil Biology and Biochemistry 43, 1812–1836.

Lehndorff, E., Wolf, M., Litt, T., Brauer, A., Amelung, W., 2015. 15,000 years of black carbon deposition – a post-glacial fire record from maar lake sediments (Germany). Quaternary Science Reviews 110, 15–22.

Leonowicz, A., Cho, N.S., Luterek, J., 2001. Fungal laccase: properties and activity on lignin. Journal of Basic Microbiology 41, 185–227.

Liang, B., Lehmann, J., Sohi, S., Thies, J., O'Neill, B., Trujillo, L., Gaunt, J., Solomon, D., Grossman, J., Neves, E., Luizão, F., 2010. Black carbon affects the cycling of non-black carbon in soil. Organic Geochemistry 41, 206–213.

Liu, Z., Demisie, W., Zhang, M., 2013. Simulated degradation of biochar and its potential environmental implications. Environmental Pollution 179, 146–152.

Luo, Y., Durenkamp, M., De Nobili, M., Lin, Q., Brookes, P.C., 2011. Short term soil priming effects and the mineralisation of biochar following its incorporation to soils of different pH. Soil Biology and Biochemistry 43, 2304–2314.

Maestrini, B., Nannipieri, P., Abiven, S., 2014a. A meta-analysis on pyrogenic organic matter induced priming effect. GCB Bioenergy 7, 577–590.

Maestrini, B., Herrmann, A.M., Nannipieri, P., Schmidt, M.W.I., Abiven, S., 2014b. Ryegrass-derived pyrogenic organic matter changes organic carbon and nitrogen mineralization in a temperate forest soil. Soil Biology and Biochemistry 69, 291–301.

Mao, J.D., Johnson, R.L., Lehmann, J., Olk, D.C., Neves, E.G., Thompson, M.L., Schmidt-Rohr, K., 2012. Abundant and stable char residues in soils: implications for soil fertility and carbon sequestration. Environmental Science and Technology 46, 9571–9576.

Márquez-Rocha, F.J., Hernández-Rodríguez, V.Z., Vázquez-Duhalt, R., 2000. Biodegradation of soil-adsorbed polycyclic aromatic hydrocarbons by the white rot fungus *Pleurotus ostreatus*. Biotechnology Letters 22, 469–472.

Masiello, C.A., Chen, Y., Gao, X., Liu, S., 2013. Biochar and microbial signaling: production conditions determine effects on microbial communication. Environmental Science and Technology 47, 11496–11503.
McHenry, M.P., 2009. Agricultural bio-char production, renewable energy generation and farm carbon sequestration in Western Australia: certainty, uncertainty and risk. Agriculture, Ecosystems and Environment 129, 1–7.
McKenna, E., Andreas, A., 1997. South Park mountain data: South Park, Colorado (data). NREL Report No. DA-5500-56521. <http://dx.doi.org/10.5439/1052562>.
Nguyen, B.T., Lehmann, J., Kinyangi, J., Smernik, R., Riha, S.J., Engelhard, M.H., 2009. Long-term black carbon dynamics in cultivated soil. Biogeochemistry 92, 163–176.
Randles, C.A., Colarco, P.R., Silva, A.D., 2013. Direct and semi-direct aerosol effects in the NASA GEOS-5 AGCM: aerosol–climate interactions due to prognostic versus prescribed aerosols. Journal of Geophysical Research: Atmospheres 118, 149–169.
Santos, F., Torn, M., Bird, J., 2012. Biological degradation of pyrogenic organic matter in temperate forest soils. Soil Biology and Biochemistry 51, 115–124.
Santos, F., Fraser, M.P., Bird, J.A., 2014. Atmospheric black carbon deposition and characterization of biomass burning tracers in a northern temperate forest. Atmospheric Environment 95, 383–390.
Schmidt, M.W.I., Skjemstad, J.O., Gehrt, E., Kögel-Knabner, I., 1999. Charred organic carbon in German chernozemic soils. European Journal of Soil Science 50, 351–365.
Schreiner, K.M., Filley, T.R., Blanchette, R.A., Bowen, B.B., Bolskar, R.D., Hockaday, W. C., Masiello, C.A., Raebiger, J.W., 2009. White-rot basidiomycete-mediated decomposition of C_{60} fullerol. Environmental Science and Technology 43, 3162–3168.
Singh, B.P., Cowie, A.L., Smernik, R.J., 2012. Biochar carbon stability in a clayey soil as a function of feedstock and pyrolysis temperature. Environmental Science and Technology 46, 11770–11778.
Skjemstad, J.O., Clarke, P., Taylor, J.A., Oades, J.M., McClure, S.G., 1996. The chemistry and nature of protected carbon in soil. Soil Research 34, 251–271.
Skjemstad, J.O., Reicosky, D.C., Wilts, A.R., McGowan, J.A., 2002. Charcoal carbon in US agricultural soils. Soil Science Society of America Journal 66, 1249–1255.
Woolf, D., Lehmann, J., 2012. Modelling the long-term response to positive and negative priming of soil organic carbon by black carbon. Biogeochemistry 111, 83–95.
Wu, C., Liu, X., Wei, D., Fan, J., Wang, L., 2001. Photosonochemical degradation of phenol in water. Water Research 35, 3927–3933.
Yao, F.X., Arbestain, M.C., Virgel, S., Blanco, F., Arostegui, J., Maciá-Agulló, J.A., Macías, F., 2010. Simulated geochemical weathering of a mineral ash-rich biochar in a modified Soxhlet reactor. Chemosphere 80, 724–732.
Zhang, F., Yu, J., 2000. Decolourisation of Acid Violet 7 with complex pellets of white rot fungus and activated carbon. Bioprocess Engineering 23, 295–301.
Zimmerman, A.R., 2010. Abiotic and microbial oxidation of laboratory-produced black carbon (biochar). Environmental Science and Technology 44, 1295–1301.
Zimmerman, A.R., Gao, B., Ahn, M.Y., 2011. Positive and negative carbon mineralization priming effects among a variety of biochar-amended soils. Soil Biology and Biochemistry 43, 1169–1179.